Available online at www.sciencedirect.com

ScienceDirect

www.elsevier.com/locate/jes

JES JOURNAL OF ENVIRONMENTAL SCIENCES

www.jesc.ac.cn

Infrared spectroscopic probing of dimethylamine clusters in an Ar matrix

Siyang Li[1], *Henrik G. Kjaergaard*[2], *Lin Du*[1,2,*]

1. *Environment Research Institute, Shandong University, Shanda South Road 27, Shandong 250100, China. E-mail: siyangli.cn@hotmail.com*
2. *Department of Chemistry, University of Copenhagen, Universitetsparken 5, DK-2100 Copenhagen Ø, Denmark*

ARTICLE INFO

Article history:
Received 30 April 2015
Revised 10 September 2015
Accepted 14 September 2015
Available online 28 December 2015

Keywords:
Matrix isolation
Infrared (IR) spectroscopy
Dimethylamine clusters
Aerosol nucleation

ABSTRACT

Amines have many atmospheric sources and their clusters play an important role in aerosol nucleation processes. Clusters of a typical amine, dimethylamine (DMA), of different sizes were measured with matrix isolation IR (infrared) and NIR (near infrared) spectroscopy. The NIR vibrations are more separated and therefore it is easier to distinguish different sizes of clusters in this region. The DMA clusters, up to DMA tetramer, have been optimized using density functional methods, and the geometries, binding energies and thermodynamic properties of DMA clusters were obtained. The computed frequencies and intensities of NH-stretching vibrations in the DMA clusters were used to interpret the experimental spectra. We have identified the fundamental transitions of the bonded NH-stretching vibration and the first overtone transitions of the bonded and free NH-stretching vibration in the DMA clusters. Based on the changes in vibrational intensities during the annealing processes, the growth of clusters was clearly observed. The results of annealing processes indicate that DMA molecules tend to form larger clusters with lower energies under matrix temperatures, which is also supported by the calculated reaction energies of cluster formation.

Introduction

It is generally accepted that aerosol particles have a great impact on global climate change, atmospheric visibility and human health (Kulmala et al., 2013; Smith et al., 2010). However, the chemical formation mechanism at the molecular level remains ambiguous and poorly understood (Zhang et al., 2012). Amines, with an odor like ammonia, are typical air pollutants in the atmosphere (Ge et al., 2011; Hellén et al., 2014). Amines can form gas clusters via hydrogen bonds or bound ion pairs and have been proposed to play a crucial role in the initial steps of aerosol nucleation according to field, modeling and laboratory studies (VandenBoer et al., 2011; Yu et al., 2012; Zhang, 2010; Zheng et al., 2015). It has been suggested that the participation of amines is a necessary process to stabilize the original clusters and decrease evaporation (Loukonen et al., 2010). Recently, research on particle nucleation of amines and sulfuric acid has been an active field in atmospheric chemistry. Kulmala et al. (2007) observed that ammonia was involved in the formation of atmospheric aerosol particles in the boreal forest in Finland. Based on quantum chemical calculations, Kurtén et al. (2008) reported subsequently that amines might enhance atmospheric sulfuric acid nucleation more effectively than ammonia. The CLOUD (Cosmics Leaving Outdoor Droplets) chamber experiments by Almeida et al. (2013) suggested that amines, especially

* *Corresponding author*. E-mail: lindu@sdu.edu.cn (Lin Du).

http://dx.doi.org/10.1016/j.jes.2015.09.012

dimethylamine (DMA), can reinforce the particle formation rates over 1000 times compared with ammonia, which supports the theoretical prediction. The formation of acid–base pairs where protons transfer from each sulfuric acid molecule to nitrogen atoms can explain the rapid nucleation (Hunter and Lias, 1998). Dimethylamine (DMA) is commonly considered as a representative amine, due to both its basicity and the number of hydrogen bonds it can form. Clusters including 14 sulfuric acid and 16 DMA molecules were observed in real time under atmospheric conditions by Kürten et al. (2014). They summarized that clusters containing one or two DMA molecules with two sulfuric acid molecules are the smallest stable structures against evaporation. In comparison with ammonia, methylamine (MA) and trimethylamine (TMA), the sulfuric acid dimer with DMA was found to be the most stable (Jen et al., 2014).

It is of critical importance to investigate small neutral clusters as they grow from monomers to ultrafine particles (Kulmala et al., 2013). Molecular dimer and larger clusters are natural ingredients in the atmosphere (Curtiss and Blander, 1988). Hydrogen bonding is an important phenomenon in many chemical and biological systems and has been studied a great deal by experimental and theoretical methods (Arunan et al., 2011). Combined with other small molecules or acids such as water and methanesulfonic acid (Bork et al., 2014b; Dawson et al., 2012, 2014; DePalma et al., 2014), DMA clusters have been proposed as pre-nucleation structures. However, their detection in the atmosphere remains elusive. The significance of these hydrogen-bonded DMA clusters is evident in atmospheric chemistry; however, despite this, relatively few laboratory investigations exist.

DMA dimer has been studied by theoretical methods, but only recently has the first spectroscopic evidence for DMA dimer at room temperature in the gas phase been reported (Du and Kjaergaard, 2011). DMA trimers have been investigated in theoretical calculations (Cabaleiro-Lago and Ríos, 2000). In addition, there is an experimental report of the electric deflection and Stark effects of DMA trimer and tetramer at low temperature (Odutola et al., 1979). The measurements of $(DMA)_n$ ($n > 2$) in the gas phase at room temperature are unfeasible. Matrix isolation IR (infrared) spectroscopy, where the molecules of interest can be trapped in a solid Ar matrix at low temperature, has shown to be an applicable technique for the probing of clusters (Ceponkus et al., 2011; Gadre et al., 2014). By controlling the mixing ratio of the matrix, more clusters and larger clusters can form. The growth of the clusters can be controlled by annealing after deposition. In the IR spectrum, overlap between fundamental transitions in different clusters makes it hard to resolve bands from the different clusters. In the near infrared (NIR) spectrum, which shows spectral features in the overtone region, differences between clusters are more easily observed, because the overtone transitions are better separated (Henry et al., 1993).

In this work, we have measured the NH-stretching fundamental and first overtone transitions of DMA clusters in the IR and NIR regions, respectively. Quantum chemical calculations of DMA clusters were performed to support the assignment of the observed spectra. The geometry and complexation energy for the DMA clusters was determined with B3LYP, M06-2X and B3LYP-D3 methods. This information can validate the importance of DMA clusters in aerosol formation and growth, and can also elucidate the contributions of DMA to nucleation events in field observation.

1. Experimental methods

The matrix isolation spectra were measured with a newly built matrix isolation Fourier Transform infrared spectroscopy (FTIR) setup (Hansen et al., 2014). The IR spectra were recorded with a Bruker Vertex 70 FTIR spectrometer fitted with a CaF_2 beam splitter. The IR spectra in the fundamental NH-stretching region were measured at 0.5 cm^{-1} resolution with 256 scans, and the NIR spectra were measured at 1 cm^{-1} resolution with 200 scans. An MCT and InGaAs detector was used to record IR and NIR spectra, respectively. Gaseous anhydrous DMA (≥99%, Aldrich, USA) was used without any further purification.

Low temperature was achieved using a closed cycle helium compressor-cooled cryostat (CS202SI, Advanced Research Systems, Inc., USA). The cryostat was housed in a vacuum chamber with base pressure $<5 \times 10^{-6}$ Torr. The pressure inside the chamber was monitored by a compact full range gauge (PKR 250, Balzers, Germany). High purity Ar gas (≥99.999%, Air Liquid, France) was used as the matrix gas. The DMA/Ar mixtures with different sample-to-matrix ratios were prepared in a 1 L glass bulb at room temperature using a vacuum line (base pressure less than 1×10^{-4} Torr). We used DMA/Ar ratios ranging from 1/45 to 1/150. The gas mixture was then deposited onto a CaF_2 substrate maintained at 12 K. The temperature of the substrate was measured with a Silicon diode sensor (Lake Shore, USA) and regulated by a temperature controller (model 32, Cryocon, USA). The flow of the gas deposition was controlled by a leak valve (model 203021, Brooks, USA). The deposition was performed at a rate of ~17 mmol/hr and lasted for about 75 min. Subsequently the matrix was slowly warmed to 25, 30 or 35 K and maintained at the temperature for 20 min, then cooled to 12 K again. The spectrum was recorded after each annealing process.

2. Computational methods

All calculations were performed using the Gaussian 09 program (Revision D.01) (Frisch et al., 2013). The structures of DMA and its dimer ($(DMA)_2$), trimer ($(DMA)_3$) and tetramer ($(DMA)_4$) were optimized with the B3LYP, M06-2X and B3LYP-D3 methods combined with the aug-cc-pVTZ basis set. Harmonic vibrational frequency calculations were performed to confirm that there were no imaginary frequencies. The M06-2X functional was found to be an excellent choice, with good accuracy in predicting the binding energies (Du et al., 2012; Hohenstein et al., 2008; Zhao and Truhlar, 2008). The popular B3LYP functional was chosen on the basis of its good performance in geometry prediction (Thanthiriwatte et al., 2011). In general, the complexes calculated by density functional theory (DFT) method are assumed to be too weakly bound. The B3LYP-D3 method adds a dispersion correction to the B3LYP DFT method (DiLabio et al., 2013; Grimme, 2011). The DFT calculations were run with the "opt = very tight" and "int = ultrafine" options. We calculated the enthalpies and Gibbs free energies (ΔH^0_{298K} and ΔG^0_{298K}) of DMA cluster formation. The complexation energy was estimated

from the complex energy minus the sum of the monomer energies, $\Delta E = E(A\cdots B) - E(A) - E(B)$. The result was subsequently corrected by zero point vibrational energy (ZPVE). The basis set superposition error (BSSE) was not computed here, because the basis-set related error for large basis sets, such as aug-cc-pVTZ, is assumed to be exaggerated by the typical counterpoise (CP) approach (Dunn et al., 2004; Feller, 1992).

The NH-stretching transition frequencies and oscillator strengths for DMA and its clusters were calculated with an anharmonic oscillator local mode model (Howard et al., 2005; Kjaergaard et al., 1990). We assumed that the NH-stretching vibration can be described by a Morse oscillator, with the vibrational energy levels given by

$$E(v)/(hc) = \left(v+\frac{1}{2}\right)\tilde{\omega} - \left(v+\frac{1}{2}\right)^2 \tilde{\omega}x. \quad (1)$$

The Morse oscillator frequency $\tilde{\omega}$ and anharmonicity $\tilde{\omega}x$ are found from the 2nd, 3rd and 4th-order derivatives of the potential energy curve (Howard et al., 2005). We obtained the 9-point potential energy curve by displacing the NH bond from −0.20 to 0.20 Å in 0.05 Å steps around the equilibrium bond length. The dimensionless oscillator strength f of a transition from the ground vibrational state to the excited vibrational state is calculated by the transition frequencies and the transition dipole moment matrix. More details of the local mode method can be found elsewhere (Low and Kjaergaard, 1999; Schofield and Kjaergaard, 2003). The calculated fundamental and overtone transition frequencies and intensities facilitate the assignment of the observed bands to DMA and its clusters.

3. Results and discussion

3.1. Geometry

Recently, we optimized the two geometries of $(DMA)_2$ (Du and Kjaergaard, 2011). The structure of $(DMA)_3$ was selected based on experimental evidence and previous computational study (Cabaleiro-Lago and Ríos, 2000; Odutola et al., 1979). Odutola et al. (1979) studied the electric deflection of DMA clusters experimentally and found that $(DMA)_3$ and $(DMA)_4$ were both nonpolar on the basis of measured Stark effects, so cyclic structures are to be expected. Many polar and linear structures of $(DMA)_3$ have been ruled out on the grounds of insufficient experimental evidence (Janeiro-Barral and Mella, 2006; Odutola et al., 1979). We further optimized the two previously determined minima on the potential energy surface for the DMA trimer (Cabaleiro-Lago and Ríos, 2000).

The most stable geometries for water tetramer and ammonia tetramer were reported to be cyclic structures (Beu and Buck, 2001; Dunn et al., 2004; Gadre et al., 2014; Lee et al., 2000; Park, 2000). $(DMA)_4$ was measured to be nonpolar and expected to be cyclic (Odutola et al., 1979). The most stable structure for $(DMA)_3$ is also cyclic (Cabaleiro-Lago and Ríos, 2000). We performed the computational study of $(DMA)_4$ for the first time and tentatively predicted that the geometry of the global minimum of $(DMA)_4$ is cyclic, planar and symmetric on the basis of the previous studies. This structure was used to aid in the assignment of the spectra, and other possible structures such as a linear structure were not considered here.

We fully optimized the DMA clusters using B3LYP, M06-2X and B3LYP-D3 functionals. We found that, for a given conformer of $(DMA)_3$ or $(DMA)_4$, the structures optimized by B3LYP and B3LYP-D3 functionals are similar; however, the M06-2X method gives a slightly different structure. The structures of DMA clusters optimized by the B3LYP functional are illustrated in Fig. 1. Two stable conformers of $(DMA)_2$ and $(DMA)_3$ were identified by our theoretical calculation. The difference between the two $(DMA)_2$ structures is that the hydrogen bond donor DMA molecule is rotated about the N···N axis. Both $(DMA)_{3A}$ and $(DMA)_{3B}$ are cyclic and differ in the position of one of the DMA molecules. In $(DMA)_{3A}$, the three molecules are equivalent and form a ring via hydrogen bonds. In $(DMA)_{3B}$, one of the DMA molecules has its N–H group pointing outside the ring, so it cannot take part in forming hydrogen bonds and this structure is not as strongly bound as $(DMA)_{3A}$. In $(DMA)_4$, the four DMA molecules are arranged similarly to those in $(DMA)_{3A}$ to form a symmetrical ring via hydrogen bonds.

The calculated N–H bond lengths, hydrogen bond lengths and hydrogen bond angles (N–H···N angles) of DMA clusters at the B3LYP/aug-cc-pVTZ level are shown in Table 1. The geometric parameters obtained with M06-2X and B3LYP-D3 functionals are given in the supplementary data. Ideally, the hydrogen bond angle in a hydrogen bonded complex is 180° (Arunan et al., 2011). The hydrogen bond angles in the majority of DMA complexes except $(DMA)_{3A}$ are close to linear, with deviation in the 6–22° range. The hydrogen bonded N–H bond lengths increase and the hydrogen bond lengths decline with DMA cluster growth. Longer N–H bond length and shorter H···N distance indicate that stronger hydrogen bonds are formed. For DMA tetramer, the N–H bond length is 1.0213 Å, which is the longest among the DMA clusters, and the hydrogen bond distance of 2.1850 Å is the shortest among them.

3.2. Thermochemistry

In relation to the individual molecule, the properties of the molecules in DMA clusters change remarkably (Yin and Landau, 2011). The thermodynamics that rules the formation of DMA clusters is the main focus here. We have calculated the energies for each incremental reaction of a DMA molecule with successive DMA clusters. The electronic energies (ΔE_0), the sum of the electronic and zero-point vibrational energies (ΔE_0 (ZPVE corrected)), the enthalpies and the Gibbs free energies (at 12 and 298 K) for the formation of the various DMA clusters computed with the M06-2X method are presented in Table 2. The results obtained with other methods are listed in the supplementary data.

DMA is a good hydrogen bond acceptor with its nitrogen atom and a relatively weak hydrogen bond donor, and can form a weak N–H···N hydrogen bond (Hunter, 2004). Under suitable conditions, DMA molecules prefer to combine with each other to form large clusters. For the DMA clusters, the stabilization effect associated with the addition of one more DMA molecule to DMA monomer, dimer or trimer is on the order of 17.0–29.7 kJ/mol with respect to ΔE_0 (ZPVE corrected),

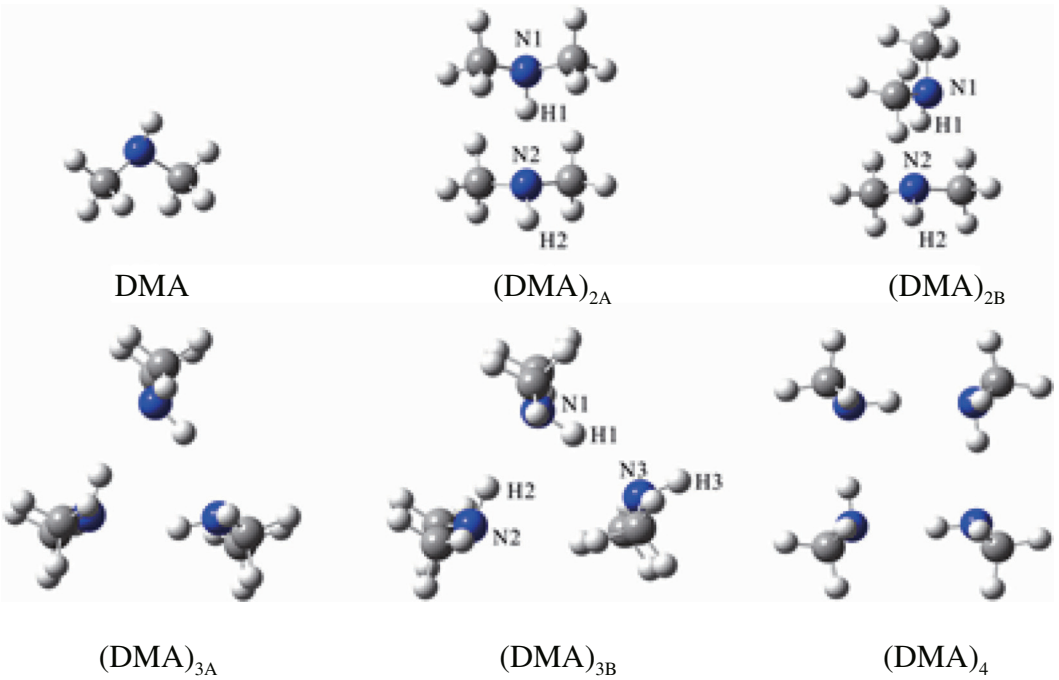

Fig. 1 – Structures of dimethylamine (DMA) and its clusters optimized by B3LYP functional.

calculated with the M06-2X functional. M06-2X and B3LYP-D3 functionals show good performance in the prediction of enthalpy (Bork et al., 2014a; Du et al., 2012; Elm et al., 2012, 2013). The enthalpy of $(DMA)_{2A}$ calculated by M06-2X is –15.3 kJ/mol at 298 K. The ΔH^0_{298K} for the formation of $(DMA)_{2A}$ by the B3LYP-D3 functional is –15.7 kJ/mol (see Appendix A. Supplementary data). The incremental enthalpy of $(DMA)_{3A}$ and $(DMA)_4$ calculated with the M06-2X functional at 298 K is –24.0 and –27.6 kJ/mol, respectively. The incremental enthalpy is larger when the cluster is larger. The results with the B3LYP-D3 functional also show the consistent change of DMA clusters. As seen in Table 2, the calculated incremental enthalpies at 12 and 298 K are quite close to each other. In water clusters, the stabilization changes calculated with G2, G3, CBS-Q3, and CBS-APNO methods are consistent (Dunn et al., 2004). For the CBS-Q3 method, the incremental enthalpy of water clusters at 298 K from monomer to tetramer is –14.2, –30.4 and –39.8 kJ/mol, respectively. It is interesting to note that the incremental enthalpy of $(DMA)_{3A}$ formation obtained by the B3LYP functional is smaller than that of $(DMA)_4$ formation (Table S3). The number of hydrogen bonds makes the difference in the formation energy between $(DMA)_{3A}$ and $(DMA)_{3B}$. The calculated Gibbs free energies at 12 and 298 K show clearly the temperature effect. At the much lower temperature of 12 K, the incremental Gibbs free energy becomes negative, and more negative for the larger clusters. As mentioned above, more hydrogen bonds can strengthen the stability of DMA clusters. They all indicate stabilization enhancement with the increase of DMA clusters. Overall, it can be concluded that it is easier to release more energy to form larger clusters.

Table 1 – N–H bond length, hydrogen bond distance and hydrogen bond angle in dimethylamine (DMA) clusters calculated at the B3LYP/aug-cc-pVTZ level.

		N–H bond length (Å)	H···N distance (Å)	N–H···N angle (degree)
DMA		1.0112		
$(DMA)_{2A}$	N1–H1	1.0162	2.2728	169.3
$(DMA)_{2B}$	N1–H1	1.0160	2.2912	171.5
$(DMA)_{3A}$		1.0186	2.2613	158.1
$(DMA)_{3B}$	N1–H1	1.0190	2.2209	170.0
	N2–H2	1.0181	2.2482	169.5
$(DMA)_4$		1.0213	2.1850	174.3

$(DMA)_4$, $(DMA)_{2A}$, $(DMA)_{2B}$, $(DMA)_{3A}$, and $(DMA)_{3B}$ refer to Fig. 1.

3.3. Frequencies and intensities

The calculated and experimental frequencies and intensities of NH-stretching for all the DMA clusters are given in Table 3. The results of both the normal mode and anharmonic oscillator local mode calculations at the B3LYP/aug-cc-pVTZ level are summarized. The normal mode results with other functionals are given in Appendix A. Supplementary data. The NH-stretching overtones are only available through anharmonic oscillator local mode calculations. The frequency and intensity for DMA monomer are in good agreement with those reported earlier (Du et al., 2013; Miller et al., 2012). For $(DMA)_{2A}$, the vibrational frequency of the N1–H1 stretching mode is 3444 cm^{-1} in the normal mode and 3275 cm^{-1} in the local mode calculation. For the DMA clusters, the agreement between the calculated values and the experiment results is not as good as it is in the isolated DMA molecule, due to couplings to lower frequency modes left out in the local mode calculation (Kjaergaard et al., 2008; Mackeprang et al., 2014, 2015). The measured NH-stretching fundamental and overtone frequencies are consistent with the calculated results in Table 3.

Table 2 – Electronic energies (ΔE_0), enthalpies (ΔH^0), and Gibbs free energies (ΔG^0) computed for the DMA cluster formation reactions at the M06-2X/aug-cc-pVTZ level (units: kJ/mol).

Reaction	ΔE_0	ΔE_0 (ZPVE corrected)	ΔH^θ_{298K}	ΔH^θ_{12K}	ΔG^θ_{298K}	ΔG^θ_{12K}
DMA + DMA ↔ $(DMA)_{2A}$	−21.4	−17.0	−15.3	−18.7	20.8	−17.4
$(DMA)_{2A}$ + DMA ↔ $(DMA)_{3A}$	−30.3	−25.8	−24.0	−23.5	16.1	−22.0
$(DMA)_{2A}$ + DMA ↔ $(DMA)_{3B}$	−24.5	−21.7	−18.9	−19.0	15.8	−17.6
$(DMA)_{3A}$ + DMA ↔ $(DMA)_4$ *	−32.1	−29.7	−27.6	−29.6	14.1	−28.0

ZPVE: zero point vibrational energy.
* Calculated without "opt = very tight" and "int = ultrafine".

As seen in Table 3, for the fundamental and first overtone transitions in the DMA clusters, the free NH-stretching frequencies are significantly larger than the bonded ones. It is worthy to note that the bonded NH-stretching fundamental transition frequency in $(DMA)_4$ (3171 cm^{-1}) is the smallest among the fundamental transitions. This indicates that the largest red shift of NH-stretching transition occurs in $(DMA)_4$.

For the DMA monomer, the fundamental NH-stretching transition intensity is weaker than the first NH-stretching overtone (Miller et al., 2012). For the DMA dimer, the fundamental transition intensity of the bonded NH-stretching is much stronger than that of the free NH-stretching. In $(DMA)_{2A}$, the bonded NH-stretching fundamental transition intensity is calculated to be 10^4 times stronger than the corresponding free NH-stretching transition. This phenomenon also exists for the two bonded and one free N–H bond of $(DMA)_{3B}$. The intensity ratio between the bonded N–H bond and free N–H bond in $(DMA)_{3B}$ is about 10^3. However, NH-stretching first overtones in DMA clusters show the opposite trend. The intensities of the bonded NH-stretching overtones are commonly weaker than those of free NH-stretching. The free NH-stretching overtone in $(DMA)_{2A}$ is about 40 times more intense than the bonded NH-stretching overtone. With the growth of DMA clusters, the intensities of bonded and free NH-stretching also enhance on the whole. The intensity of the bonded NH-stretching in $(DMA)_{3B}$ (N1–H1) is calculated to be 5.9×10^{-5}, which is slightly larger than the corresponding intensity in $(DMA)_{2B}$ (4.7×10^{-5}). The intensity of free NH-stretching increases by a factor of 1.5 from $(DMA)_{2B}$ to $(DMA)_{3B}$.

Table 3 – Measured and calculated NH-stretching fundamental and overtone frequencies ($\tilde{\upsilon}$) and oscillator strengths (f).

Cluster		υ	Experimental			Calculated [a]				
			Gas		Matrix	Local mode		Normal mode		
			$\tilde{\upsilon}$ (cm^{-1})	f	$\tilde{\upsilon}$ (cm^{-1})	$\tilde{\upsilon}$ (cm^{-1})	f	$\tilde{\upsilon}$ (cm^{-1})	f	f_{total}
DMA	$(N–H)_f$	1	3359, 3374 [b]	1.0×10^{-7} [b]	3377	3379	5.3×10^{-8}	3527	1.1×10^{-7}	1.1×10^{-7}
$(DMA)_{2A}$	$(N1–H1)_b$	1	3339 [c]		3304	3275	4.6×10^{-5}	3444	3.9×10^{-5}	3.9×10^{-5}
$(DMA)_{2A}$	$(N2–H2)_f$	1				3373	4.4×10^{-9}	3520	1.7×10^{-7}	
$(DMA)_{2B}$	$(N1–H1)_b$	1			3313	3278	4.7×10^{-5}	3445	3.9×10^{-5}	3.9×10^{-5}
$(DMA)_{2B}$	$(N2–H2)_f$	1				3372	3.7×10^{-8}	3517	1.7×10^{-7}	
$(DMA)_{3A}$	$(N–H)_b$	1			3246	3203	1.7×10^{-5}	3412	6.3×10^{-5}	1.3×10^{-4}
	$(N–H)_b$	1						3395	0	
$(DMA)_{3B}$	$(N1–H1)_b$	1			3282	3221	5.9×10^{-5}	3396	4.1×10^{-5}	
$(DMA)_{3B}$	$(N2–H2)_b$	1			3294	3233	5.7×10^{-5}	3414	5.3×10^{-5}	9.4×10^{-5}
$(DMA)_{3B}$	$(N3–H3)_f$	1				3366	5.7×10^{-8}	3512	8.0×10^{-8}	
$(DMA)_4$	$(N–H)_b$	1			3215	3171	8.4×10^{-5}	3362	1.3×10^{-4}	
	$(N–H)_b$	1						3371	0	2.6×10^{-4}
	$(N–H)_b$	1						3340	0	
DMA	$(N–H)_f$	2	6579, 6591 [b]	5.5×10^{-7} [b]	6596	6607	4.4×10^{-7}			
$(DMA)_{2A}$	$(N1–H1)_b$	2			6465	6382	1.0×10^{-8}			
$(DMA)_{2A}$	$(N2–H2)_f$	2			6581	6595	4.1×10^{-7}			
$(DMA)_{2B}$	$(N1–H1)_b$	2			6465	6388	1.4×10^{-8}			
$(DMA)_{2B}$	$(N2–H2)_f$	2			6581	6594	3.8×10^{-7}			
$(DMA)_{3A}$	$(N–H)_b$	2			6207	6108	6.5×10^{-7}			
$(DMA)_{3B}$	$(N1–H1)_b$	2			6232	6264	3.1×10^{-8}			
$(DMA)_{3B}$	$(N2–H2)_b$	2			6238	6289	3.2×10^{-8}			
$(DMA)_{3B}$	$(N3–H3)_f$	2			6544	6582	4.4×10^{-7}			
$(DMA)_4$	$(N–H)_b$	2			6165	6157	6.2×10^{-8}			

$(N–H)_b$: bonded N–H hydrogen bond; $(N–H)_f$: free N–H hydrogen bond; υ: the vibrational quantum number, 1 for the NH-stretching fundamental transition and 2 for the NH-stretching first overtone transition.
[a] Calculated at the B3LYP/aug-cc-pVTZ level.
[b] Miller et al. (2012).
[c] Du and Kjaergaard (2011).

For the anharmonic local mode calculations, we ignore the coupling between DMA units in clusters. The intensities of individual N–H bonds and the total intensities for N–H bonds in DMA clusters $(DMA)_2$, $(DMA)_3$ and $(DMA)_4$ obtained by harmonic normal mode calculations are listed in Table 3 and in Appendix A. Supplementary data. The intensity of bonded fundamental NH-stretching transitions is 2 to 4 orders of magnitude larger than that of free NH-stretching, therefore the total intensity of NH-stretching in clusters depends mainly on the number of hydrogen bonds. The total intensities were added up for the transitions with the same or similar frequencies. Generally, larger clusters have larger fundamental NH-stretching total intensity. However, the first overtone of bonded NH-stretching transition is only one order of magnitude smaller than that of free NH-stretching, according to the local mode results. Both bonded and free NH-stretching transition intensity has to be taken into account when calculating the total intensity of the first overtone. For the harmonic calculation of $(DMA)_{3A}$ at the B3LYP/aug-cc-pVTZ level, two N–H bonds have the same intensities of 6.3×10^{-5}; the third one is IR non-active, therefore the total intensity adds up to 1.3×10^{-4}. Similarly, the total intensity in $(DMA)_4$ was obtained. The total intensities of NH-stretching increase with the growth of DMA clusters. The calculated frequencies and intensities for DMA clusters play a vital role in supporting the assignment of experimental matrix isolation spectra.

3.4. IR and NIR spectra and assignments

The IR spectra of the DMA monomer and clusters were measured in Ar matrixes with a DMA/Ar ratio of 5/702 and 15/719 and are shown in Figs. 2 and 3, respectively. Bands associated with NH-stretching fundamental transitions were observed. The frequencies of the observed transitions are summarized in Table 3.

Only if clusters accumulate to a certain amount and have a relative strong intensity, can they be detected by IR spectroscopy. In Fig. 2, the spectra indicate the formation of DMA clusters. The 3215, 3246, 3282, 3294, 3304, 3313 and 3377 cm^{-1}

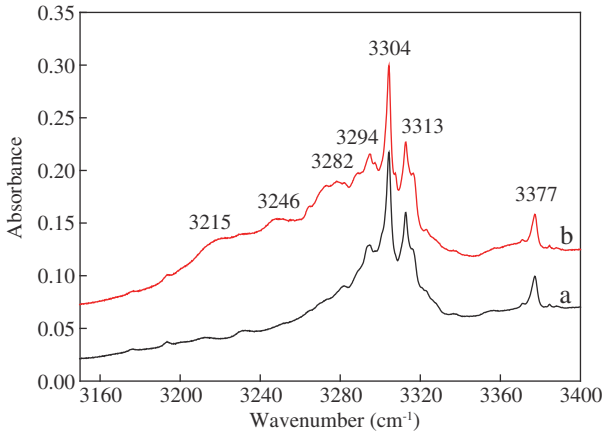

Fig. 2 – Infrared spectra of the NH-stretching fundamental transition region recorded at 12 K (a) immediately after deposition and (b) after annealing to 25 K. The mixing ratio of DMA/Ar is 5/702.

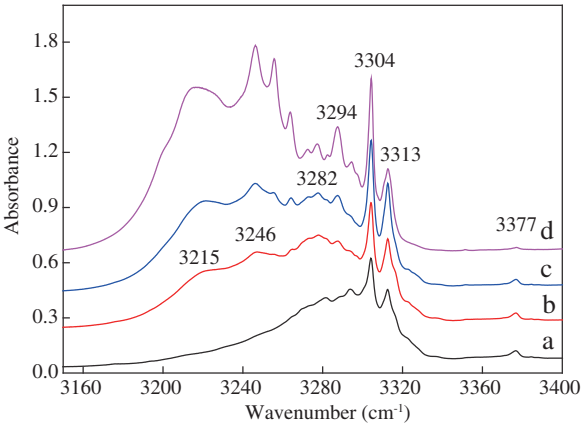

Fig. 3 – IR spectra of the NH-stretching fundamental transition region recorded at 12 K (a) immediately after deposition, (b) after annealing to 25 K, (c) after annealing to 30 K, and (d) after annealing to 35 K. The mixing ratio of DMA/Ar is 15/719. IR: infrared.

absorption were the most intense in Fig. 2. The band at 3377 cm^{-1} is assigned to the fundamental NH-stretching transition of DMA monomer, in good agreement with a previous study (Bohn and Andrews, 1991). Compared with calculated results of bonded and free NH-stretching vibrations, the corresponding frequencies of N–H bonds in DMA dimer, trimer and tetramer can be identified. As seen in Table 3, the bands at 3304 and 3313 cm^{-1} could be the bonded NH-stretching vibrations in $(DMA)_{2A}$ and $(DMA)_{2B}$, respectively. They are consistent with the values reported previously (Bohn and Andrews, 1991). The $(DMA)_{2A}$ and $(DMA)_{2B}$ absorptions at 3304 and 3313 cm^{-1} show 73 and 64 cm^{-1} red shifts from the NH-stretching absorptions of DMA in the Ar matrix, respectively. The IR spectrum of DMA dimer was obtained in the gas phase at room temperature (Du and Kjaergaard, 2011). The DMA dimer absorption at 3339 cm^{-1} is red-shifted by 35 cm^{-1} from the NH-stretching of DMA in the gas phase, which is smaller than the red shift in the Ar matrix. This can be explained by temperature effects. Hydrogen bonding is weakened by thermal excitation, which results in a much less pronounced frequency shift at room temperature (Hippler et al., 2010). The observed shift in the Ar matrix is closer to the theoretically predicted shift for DMA dimer, compared with the experimental observation at room temperature. Given the predicted much weaker intensity of the free NH-stretching vibration compared to the bonded NH-stretching vibration, the free NH-stretching vibration in the clusters was not observable in the matrix IR spectra.

To further illustrate the formation of DMA clusters, we raised the temperature to give DMA molecules more freedom to move around in the matrix and to collide with each other. Raising the proportion of DMA in an Ar matrix also facilitates the formation of larger clusters. We recorded the spectra of DMA in an Ar matrix with a mixing ratio of 15/719 for three different annealing processes for comparison. The labeled bands in Fig. 2 also exist in Fig. 3, but with a different relative intensity. The NH-stretching vibration band of $(DMA)_{2A}$ in Ar matrixes is significantly higher than that of the DMA monomer, especially for higher DMA/Ar mixing ratios. The

band at 3246 cm^{-1} present after annealing to 25 K is assigned to the bonded NH-stretching vibration in $(DMA)_{3A}$. There are two bonded N–H bonds in $(DMA)_{3B}$, which result in the two bands at 3282 and 3294 cm^{-1}, respectively. Although $(DMA)_{3B}$ is less stable than $(DMA)_{3A}$, it could still be possible to form a certain amount at the low temperature of the Ar matrix. As shown in Fig. 3, the growth of the 3294 cm^{-1} band after each annealing process indicates the formation of more clusters with $(DMA)_{3B}$ structure. The 3246 cm^{-1} band from $(DMA)_{3A}$ grows more intense than the bands at 3282 cm^{-1} after annealing (Fig. 3), which partially confirms that $(DMA)_{3A}$ is more strongly bound than $(DMA)_{3B}$. The fundamental NH-stretching transition of $(DMA)_4$ is located at about 3215 cm^{-1} in the spectrum, and becomes very strong after annealing. The red shift compared with DMA monomer is large, as predicted theoretically (Table 3), because the hydrogen bonding in $(DMA)_4$ is stronger than that in other clusters.

We measured the spectra in the region 6100–6700 cm^{-1} corresponding to the first NH-stretching overtone of a DMA/Ar mixture (15/714). Although generally the absorption is weak in the NIR region, the bands arising from the first overtones of free NH-stretching vibration (6500–6620 cm^{-1}) were observed and are shown in Fig. 4. The first overtones of N–H bonds in DMA and its clusters were observed for the first time in Ar matrix conditions. The band at 6596 cm^{-1} is assigned to the NH-stretching first overtone of DMA monomer, which is close to the position (6591 cm^{-1}) in the gas phase experiments (Miller et al., 2012). The 6596 cm^{-1} band has the strongest absorbance in the NIR region, for two reasons: there are basically very many DMA monomers in the mixture on the matrix, although part of them form larger clusters; the free NH-stretching first overtone in DMA has quite high intensity (Table 3). However, one might argue that the DMA band in Fig. 3 looks small compared with the dimer bands, under similar mixing ratio matrix conditions. This is exactly because the bonded NH-stretching transition has about 10^3 times stronger intensity than the free NH-stretching in DMA monomer. The concentration of monomer should still be larger than the dimer under the conditions in Figs. 3 and 4. The first overtones of the free NH-stretching vibration in $(DMA)_{2A}$ and $(DMA)_{2B}$ are assigned to the band at 6581 cm^{-1}. The calculated frequencies of these two transitions are quite similar to each other (Table 3), and therefore it is reasonable to believe these two bands overlap. The 6544 cm^{-1} band is assigned to the free NH-stretching vibration in $(DMA)_{3B}$. However, the 6550 and 6530 cm^{-1} bands could not be assigned definitely, but might be from free NH-stretching vibrations in other clusters. It is worthy to note that the decrease of the absorption at 6596 cm^{-1} and the obvious increase of the 6544 cm^{-1} band after the annealing processes indicated that DMA monomer was transformed into larger DMA clusters, agreeing with the conclusion shown in Fig. 3. Other bands do not change significantly enough to show a difference under this condition, due to the possible loss of molecules on the matrix in the vacuum chamber during the annealing processes.

The first overtones of free NH-stretching vibrations show a relatively stronger absorbance than the fundamental transitions. The first overtone of the bonded NH-stretching vibration is expected to be weak and difficult to measure. We tried to measure the spectra in the 6100–6500 cm^{-1} region, which is shown in Appendix A. Supplementary data. The band at 6465 cm^{-1} is assigned to the first overtones of the bonded NH-stretching vibration in $(DMA)_{2A}$ and $(DMA)_{2B}$. The first overtones of the two bonded NH-stretching vibrations in $(DMA)_{3B}$ are tentatively assigned to the weak bands at 6232 and 6238 cm^{-1}, respectively. With stronger hydrogen bonding and a larger red shift than $(DMA)_{3B}$, the first overtone of the NH-stretching vibration in $(DMA)_{3A}$ is assigned to the 6207 cm^{-1} band. The intensity of the bonded NH-stretching first overtone in $(DMA)_4$ is calculated to be a factor of 2 higher than the bonded NH-stretching in $(DMA)_{3B}$. The band at 6165 cm^{-1}, which has the largest red shift, is tentatively assigned to the first overtone of the bonded NH-stretching vibration in $(DMA)_4$. In addition, the bands in the matrix spectra might arise from spectral splitting due to the presence of different sites within the solid matrix.

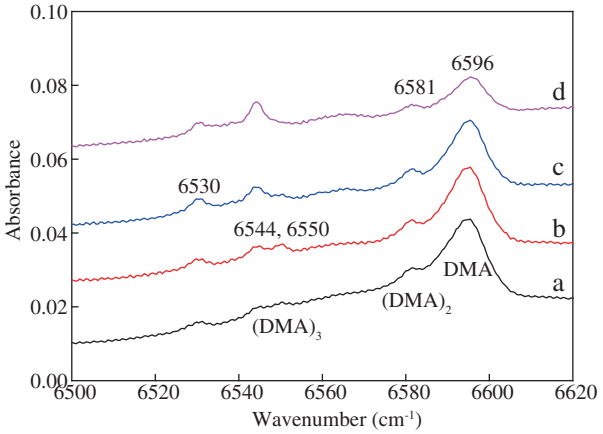

Fig. 4 – NIR (near infrared) spectra of the NH-stretching first overtone region recorded at 12 K (a) immediately after deposition, (b) after annealing to 25 K, (c) after annealing to 30 K, and (d) after annealing to 35 K. The mixing ratio of DMA/Ar is 15/714.

4. Conclusions

We have optimized the clusters of dimethylamine (DMA) by using the B3LYP, M06-2X and B3LYP-D3 functionals. The complexation energy increases with addition of each DMA molecule, indicating that formation of larger clusters releases more energy. We have observed the bands of different sizes of DMA clusters in matrix isolation IR and NIR spectroscopy. Especially in the NIR region, it is much easier to distinguish different sizes of clusters. With the help of computed frequencies and intensities, we assigned the spectra. For the NH-stretching vibrations in each DMA cluster, the first overtone bands were identified. Larger clusters form after each annealing process at three different temperatures. The good consistency between the calculated and measured results confirms that DMA molecules have a tendency to form larger clusters in the matrix. The finding supports the previous reports that DMA helps the stabilization and growth of atmospheric clusters and plays an important role in aerosol formation.

Acknowledgments

This work was supported by the Danish Council for Independent Research — Natural Sciences, the Danish Center for Scientific Computing (DCSC), National Natural Science Foundation of China (Nos. 21407095, 21577080) and Shandong Provincial Natural Science Foundation, China (No. ZR2014BQ013).

Appendix A. Supplementary data

Supplementary data to this article can be found online at http://dx.doi.org/10.1016/j.jes.2015.09.012.

REFERENCES

Almeida, J., Schobesberger, S., Kürten, A., Ortega, I.K., Kupiainen-Määttä, O., Praplan, A.P., et al., 2013. Molecular understanding of sulphuric acid-amine particle nucleation in the atmosphere. Nature 502 (7471), 359–363.

Arunan, E., Desiraju, G.R., Klein, R.A., Sadlej, J., Scheiner, S., Alkorta, I., et al., 2011. Definition of the hydrogen bond (IUPAC Recommendations 2011). Pure Appl. Chem. 83 (8), 1637–1641.

Beu, T.A., Buck, U., 2001. Structure of ammonia clusters from n = 3 to 18. J. Chem. Phys. 114 (18), 7848–7852.

Bohn, R.B., Andrews, L., 1991. FTIR spectra of ammonia–methylamine complexes in solid argon. J. Phys. Chem. 95 (24), 9707–9712.

Bork, N., Du, L., Reiman, H., Kurtén, T., Kjaergaard, H.G., 2014a. Benchmarking ab initio binding energies of hydrogen-bonded molecular clusters based on FTIR spectroscopy. J. Phys. Chem. A 118 (28), 5316–5322.

Bork, N., Elm, J., Olenius, T., Vehkamaki, H., 2014b. Methane sulfonic acid-enhanced formation of molecular clusters of sulfuric acid and dimethyl amine. Atmos. Chem. Phys. 14 (22), 12023–12030.

Cabaleiro-Lago, E.M., Ríos, M.A., 2000. An *ab initio* study of the interaction in dimethylamine dimer and trimer. J. Chem. Phys. 113 (21), 9523–9531.

Ceponkus, J., Uvdal, P., Nelander, B., 2011. On the structure of the matrix isolated water trimer. J. Chem. Phys. 134 (6), 064309.

Curtiss, L.A., Blander, M., 1988. Thermodynamic properties of gas-phase hydrogen-bonded complexes. Chem. Rev. 88 (6), 827–841.

Dawson, M.L., Varner, M.E., Perraud, V., Ezell, M.J., Gerber, R.B., Finlayson-Pitts, B.J., 2012. Simplified mechanism for new particle formation from methanesulfonic acid, amines, and water via experiments and ab initio calculations. Proc. Natl. Acad. Sci. U. S. A. 109 (46), 18719–18724.

Dawson, M.L., Varner, M.E., Perraud, V., Ezell, M.J., Wilson, J., Zelenyuk, A., et al., 2014. Amine–amine exchange in aminium–methanesulfonate aerosols. J. Phys. Chem. C 118 (50), 29431–29440.

DePalma, J.W., Doren, D.J., Johnston, M.V., 2014. Formation and growth of molecular clusters containing sulfuric acid, water, ammonia, and dimethylamine. J. Phys. Chem. A 118 (29), 5464–5473.

DiLabio, G.A., Johnson, E.R., Otero-de-la-Roza, A., 2013. Performance of conventional and dispersion-corrected density-functional theory methods for hydrogen bonding interaction energies. Phys. Chem. Chem. Phys. 15 (31), 12821–12828.

Du, L., Kjaergaard, H.G., 2011. Fourier transform infrared spectroscopy and theoretical study of dimethylamine dimer in the gas phase. J. Phys. Chem. A 115 (44), 12097–12104.

Du, L., Lane, J.R., Kjaergaard, H.G., 2012. Identification of the dimethylamine–trimethylamine complex in the gas phase. J. Chem. Phys. 136 (18), 184305.

Du, L., Mackeprang, K., Kjaergaard, H.G., 2013. Fundamental and overtone vibrational spectroscopy, enthalpy of hydrogen bond formation and equilibrium constant determination of the methanol–dimethylamine complex. Phys. Chem. Chem. Phys. 15 (25), 10194–10206.

Dunn, M.E., Pokon, E.K., Shields, G.C., 2004. Thermodynamics of forming water clusters at various temperatures and pressures by gaussian-2, gaussian-3, complete basis set-QB3, and complete basis set-APNO model chemistries; implications for atmospheric chemistry. J. Am. Chem. Soc. 126 (8), 2647–2653.

Elm, J., Bilde, M., Mikkelsen, K.V., 2012. Assessment of density functional theory in predicting structures and free energies of reaction of atmospheric prenucleation clusters. J. Chem. Theory Comput. 8 (6), 2071–2077.

Elm, J., Bilde, M., Mikkelsen, K.V., 2013. Assessment of binding energies of atmospherically relevant clusters. Phys. Chem. Chem. Phys. 15 (39), 16442–16445.

Feller, D., 1992. Application of systematic sequences of wave functions to the water dimer. J. Chem. Phys. 96 (8), 6104–6114.

Frisch, M.J., Trucks, G.W., Schlegel, H.B., Scuseria, G.E., Robb, M.A., Cheeseman, J.R., et al., 2013. Gaussian 09 (Revision D.01). Wallingford CT.

Gadre, S.R., Yeole, S.D., Sahu, N., 2014. Quantum chemical investigations on molecular clusters. Chem. Rev. 114 (24), 12132–12173.

Ge, X., Wexler, A.S., Clegg, S.L., 2011. Atmospheric amines—part I a review. Atmos. Environ. 45 (3), 524–546.

Grimme, S., 2011. Density functional theory with London dispersion corrections. Wiley Interdiscip. Rev.: Comput. Mol. Sci. 1 (2), 211–228.

Hansen, A.S., Du, L., Kjaergaard, H.G., 2014. Positively charged phosphorus as a hydrogen bond acceptor. J. Phys. Chem. Lett. 5 (23), 4225–4231.

Hellén, H., Kieloaho, A.J., Hakola, H., 2014. Gas-phase alkyl amines in urban air; comparison with a boreal forest site and importance for local atmospheric chemistry. Atmos. Environ. 94, 192–197.

Henry, B.R., Kjaergaard, H.G., Niefer, B., Schattka, B.J., Turnbull, D.M., 1993. The local mode model and recent advances in laser-based photoacoustic-spectroscopy—1992 Gerhard Herzberg Award address. Can. J. Appl. Spectrosc. 38 (2), 42–50.

Hippler, M., Hesse, S., Suhm, M.A., 2010. Quantum-chemical study and FTIR jet spectroscopy of $CHCl_3$–NH_3 association in the gas phase. Phys. Chem. Chem. Phys. 12 (41), 13555–13565.

Hohenstein, E.G., Chill, S.T., Sherrill, C.D., 2008. Assessment of the performance of the M05-2X and M06-2X exchange-correlation functionals for noncovalent interactions in biomolecules. J. Chem. Theory Comput. 4 (12), 1996–2000.

Howard, D.L., Jørgensen, P., Kjaergaard, H.G., 2005. Weak intramolecular interactions in ethylene glycol identified by vapor phase OH-stretching overtone spectroscopy. J. Am. Chem. Soc. 127 (48), 17096–17103.

Hunter, C.A., 2004. Quantifying intermolecular interactions: guidelines for the molecular recognition toolbox. Angew. Chem. Int. Ed. 43 (40), 5310–5324.

Hunter, E.P.L., Lias, S.G., 1998. Evaluated gas phase basicities and proton affinities of molecules: an update. J. Phys. Chem. Ref. Data 27 (3), 413.

Janeiro-Barral, P.E., Mella, M., 2006. Study of the structure, energetics, and vibrational properties of small ammonia clusters $(NH_3)_n$ (n = 2–5) using correlated ab initio methods. J. Phys. Chem. A 110 (39), 11244–11251.

Jen, C.N., McMurry, P.H., Hanson, D.R., 2014. Stabilization of sulfuric acid dimers by ammonia, methylamine, dimethylamine, and trimethylamine. J. Geophys. Res. Atmos. 119 (12), 7502–7514.

Kjaergaard, H.G., Yu, H., Schattka, B.J., Henry, B.R., Tarr, A.W., 1990. Intensities in local mode overtone spectra: propane. J. Chem. Phys. 93 (9), 6239–6248.
Kjaergaard, H.G., Garden, A.L., Chaban, G.M., Gerber, R.B., Matthews, D.A., Stanton, J.F., 2008. Calculation of vibrational transition frequencies and intensities in water dimer: comparison of different vibrational approaches. J. Phys. Chem. A 112 (18), 4324–4335.
Kulmala, M., Riipinen, I., Sipilä, M., Manninen, H.E., Petäjä, T., Junninen, H., et al., 2007. Toward direct measurement of atmospheric nucleation. Science 318 (5847), 89–92.
Kulmala, M., Kontkanen, J., Junninen, H., Lehtipalo, K., Manninen, H.E., Nieminen, T., et al., 2013. Direct observations of atmospheric aerosol nucleation. Science 339 (6122), 943–946.
Kurtén, T., Loukonen, V., Vehkamäki, H., Kulmala, M., 2008. Amines are likely to enhance neutral and ion-induced sulfuric acid–water nucleation in the atmosphere more effectively than ammonia. Atmos. Chem. Phys. 8 (14), 4095–4103.
Kürten, A., Jokinen, T., Simon, M., Sipilä, M., Sarnela, N., Junninen, H., et al., 2014. Neutral molecular cluster formation of sulfuric acid-dimethylamine observed in real time under atmospheric conditions. Proc. Natl. Acad. Sci. U. S. A. 111 (42), 15019–15024.
Lee, H.M., Suh, S.B., Lee, J.Y., Tarakeshwar, P., Kim, K.S., 2000. Structures, energies, vibrational spectra, and electronic properties of water monomer to decamer. J. Chem. Phys. 112 (22), 9759–9772.
Loukonen, V., Kurten, T., Ortega, I.K., Vehkamäki, H., Pádua, A.A.H., Sellegri, K., et al., 2010. Enhancing effect of dimethylamine in sulfuric acid nucleation in the presence of water-a computational study. Atmos. Chem. Phys. 10 (10), 4961–4974.
Low, G.R., Kjaergaard, H.G., 1999. Calculation of OH-stretching band intensities of the water dimer and trimer. J. Chem. Phys. 110 (18), 9104–9115.
Mackeprang, K., Kjaergaard, H.G., Salmi, T., Hänninen, V., Halonen, L., 2014. The effect of large amplitude motions on the transition frequency redshift in hydrogen bonded complexes: a physical picture. J. Chem. Phys. 140 (18), 184309.
Mackeprang, K., Hänninen, V., Halonen, L., Kjaergaard, H.G., 2015. The effect of large amplitude motions on the vibrational intensities in hydrogen bonded complexes. J. Chem. Phys. 142 (9), 094304.
Miller, B.J., Du, L., Steel, T.J., Paul, A.J., Södergren, A.H., Lane, J.R., et al., 2012. Absolute intensities of NH-stretching transitions in dimethylamine and pyrrole. J. Phys. Chem. A 116 (1), 290–296.
Odutola, J.A., Dyke, T.R., Howard, B.J., Muenter, J.S., 1979. Molecular beam electric deflection study of ammonia polymers. J. Chem. Phys. 70 (11), 4884–4886.
Park, J.K., 2000. Ab initio studies for geometrical structures of ammonia cluster cations. J. Phys. Chem. A 104 (21), 5093–5100.
Schofield, D.P., Kjaergaard, H.G., 2003. Calculated OH-stretching and HOH-bending vibrational transitions in the water dimer. Phys. Chem. Chem. Phys. 5 (15), 3100–3105.
Smith, J.N., Barsanti, K.C., Friedli, H.R., Ehn, M., Kulmala, M., Collins, D.R., et al., 2010. Observations of aminium salts in atmospheric nanoparticles and possible climatic implications. Proc. Natl. Acad. Sci. U. S. A. 107 (15), 6634–6639.
Thanthiriwatte, K.S., Hohenstein, E.G., Burns, L.A., Sherrill, C.D., 2011. Assessment of the performance of DFT and DFT-D methods for describing distance dependence of hydrogen-bonded interactions. J. Chem. Theory Comput. 7 (1), 88–96.
VandenBoer, T.C., Petroff, A., Markovic, M.Z., Murphy, J.G., 2011. Size distribution of alkyl amines in continental particulate matter and their online detection in the gas and particle phase. Atmos. Chem. Phys. 11 (9), 4319–4332.
Yin, J., Landau, D.P., 2011. Structural properties and thermodynamics of water clusters: a Wang–Landau study. J. Chem. Phys. 134 (7), 074501.
Yu, H., McGraw, R., Lee, S.H., 2012. Effects of amines on formation of sub-3 nm particles and their subsequent growth. Geophys. Res. Lett. 39 (2), L02807.
Zhang, R.Y., 2010. Getting to the critical nucleus of aerosol formation. Science 328 (5984), 1366–1367.
Zhang, R.Y., Khalizov, A., Wang, L., Hu, M., Xu, W., 2012. Nucleation and growth of nanoparticles in the atmosphere. Chem. Rev. 112 (3), 1957–2011.
Zhao, Y., Truhlar, D.G., 2008. Density functionals with broad applicability in chemistry. Acc. Chem. Res. 41 (2), 157–167.
Zheng, J., Ma, Y., Chen, M.D., Zhang, Q., Wang, L., Khalizov, A.F., et al., 2015. Measurement of atmospheric amines and ammonia using the high resolution time-of-flight chemical ionization mass spectrometry. Atmos. Environ. 102, 249–259.